Final report on

Theoretical prediction of the hypersonic boundary layer over a row of microcavities

September, 2002

by

Peter W. Duck[†]
1 Bower Road, Hale, Cheshire, WA15 9DT, ENGLAND

1 Background

The preliminary report on this contract (submitted in January 2002) described the potential of microcavities stabilizing hypersonic flows, especially with respect to the second mode of instability - the dominant source of flow transition in this regime. This work was presented at the 3rd AIAA Theoretical Fluid Mechanics Meeting in St Louis in June, and an offprint of the paper (AIAA 2002-2987) is attached as an appendix to this final report. The first phase of the work was partly concerned with the nature of the flow inside each individual microcavity, and it was shown that this could be regarded as incompressible and highly viscous. This result was exploited in the the associated work of Theofilis (performed under EOARD/USAF Contract No. F61775-01-WE049) which focused mainly on the flow inside a microcavity in which the nature of the basic flow was modeled as that inside a single cavity, driven by a uniform shear on the (upper) boundary. As such, this model may be regarded as a modification of the classical lid-driven cavity problem of Burggraf [1], with a single modified boundary condition. This work also indicated that the flow inside each microcavity was exceedingly stable, i.e. flow instabilities inside each microcavity are not an issue.

Other work performed in the first phase of this contract focused on the (inviscid) stability of the outer (boundary-layer) flow, modeling the wall porosity by means of a modified wall boundary condition, linking the normal velocity component on the wall to the wall pressure. This indicated strongly, that there certainly exists a significant potential for flow stabilization, over a very broad range of parameters. Typically reductions in growth rates of circa 50% seem to be (easily) possible, and this is in surprisingly good quantitative agreement with the experimental work of Rasheed et al. [2] (whilst also confirming the theoretical work of [3]).

[†]This material is based upon work supported by the European Office of Aerospace Research and Development, Air Force Office of Scientific Research, Air Force Research Laboratory, under Contract No. F61775-01-WE046 monitored by Dr. Steven Walker

REPORT DOCUMENTATION PAGE

Form Approved OMB No. 0704-0188

1. REPORT DATE *(DD-MM-YYYY)*	2. REPORT TYPE	3. DATES COVERED *(From – To)*
22-10-2002	Final Report	13 June 2001 - 13-Jun-02

4. TITLE AND SUBTITLE

Theoretical prediction of the hypersonic boundary-layer over a row of microcavities

5a. CONTRACT NUMBER
F61775-01-WE046

5b. GRANT NUMBER

5c. PROGRAM ELEMENT NUMBER

6. AUTHOR(S)

Dr. Peter Duck

5d. PROJECT NUMBER

5d. TASK NUMBER

5e. WORK UNIT NUMBER

7. PERFORMING ORGANIZATION NAME(S) AND ADDRESS(ES)
University of Manchester
Manchester M13 9PL
United Kingdom

8. PERFORMING ORGANIZATION REPORT NUMBER
N/A

9. SPONSORING/MONITORING AGENCY NAME(S) AND ADDRESS(ES)

EOARD
PSC 802 BOX 14
FPO 09499-0014

10. SPONSOR/MONITOR'S ACRONYM(S)

11. SPONSOR/MONITOR'S REPORT NUMBER(S)
SPC 01-4046

12. DISTRIBUTION/AVAILABILITY STATEMENT

Approved for public release; distribution is unlimited.

13. SUPPLEMENTARY NOTES

14. ABSTRACT

This report results from a contract tasking University of Manchester as follows: The key deliverable will be the ability to provide an improved integral condition for calculations in the main body of the flow. Given the plethora of parameters (M, Re, m, d, d/D, d/s), only a small subset of parameter space will be investigated within the available year; however a theoretical approach provides a fast means to investigate certain parameter regimes. Particular attention will be focused on the choice of (boundary) conditions to be imposed inside the cavity. Various asymptotic limits to the problem will be considered analytically, where appropriate, including the limit of very narrow and also very deep cavities. The possibility of modeling the cavity flow as incompressible will be thoroughly investigated. Also, the sensitivity of some of the underlying assumptions will be investigated. Once the 'micro' detail of the pressure field has been determined (through analytic and/or numerical means), a study will be undertaken to determine the best/most appropriate manner in which to construct a surface integral condition for use within the outer flow calculations. Progress of the proposed work will be monitored by means of one intermediate and one final report.

15. SUBJECT TERMS
EOARD, Boundary Layer, Hypersonic Flow, Aeroacoustics, Cavity Acoustics

16. SECURITY CLASSIFICATION OF:			17. LIMITATION OF ABSTRACT	18, NUMBER OF PAGES	19a. NAME OF RESPONSIBLE PERSON
a. REPORT	b. ABSTRACT	c. THIS PAGE			Wayne Donaldson
UNCLAS	UNCLAS	UNCLAS	UL		19b. TELEPHONE NUMBER *(Include area code)* +44 (0)20 7514 4299

The key issue addressed in the second phase of this work has been the linkage between the flow inside the microcavities and that in the outer (boundary-layer) flow; this final report details results related to this aspect, and also indicates the direction of other possible studies for the future.

2 Description of work performed

The outer flow

As before, taking the x coordinate in the streamwise direction, Y the normal boundary-layer coordinate (scaled with $R^{-\frac{1}{2}}$ in the usual boundary-layer manner), then the corresponding base flow (nondimensionalized with respect to the freestream velocity U_∞, which is also used in our definition of the outer Reynolds number R), and temperature field, then takes the form

$$(\mathbf{u}, T) = ((U_0(Y), 0), T_0(Y)) + O(R^{-\frac{1}{2}}), \tag{1}$$

where the use of the parallel-flow approximation is explicitly assumed, consistent with the scale of the flow disturbance field (note too that the similarity form for the compressible boundary-layer equations was used in the evaluation of the above quantities).

Small amplitude disturbances are imposed on (1) and written in the usual (normal-mode) form, i.e.

$$(\tilde{u}, \tilde{v}, \tilde{p}, \tilde{T}, \tilde{\rho}) = (\hat{u}, \alpha\hat{v}, \hat{p}, \hat{T}, \hat{\rho}) e^{iR^{\frac{1}{2}}\alpha(x-ct)}. \tag{2}$$

Here α denotes the wavenumber of the disturbance and c is the associated wavespeed. Substituting the disturbance flowfield into the inviscid, compressible equations of motion, discarding quadratic amplitude terms leads to the following system

$$-ic\hat{\rho} + \frac{i\hat{u}}{T_0} + \frac{1}{T_0}\tilde{v}_Y + iU_0\hat{\rho} + \hat{v}\frac{d}{dY}(\frac{1}{T_0}) = 0, \tag{3}$$

$$-\frac{ic}{T_0}\tilde{u} + \frac{iU_0\hat{u}}{T_0} + \frac{\hat{u}U_{0Y}}{T_0} = -\frac{i\hat{p}}{\gamma M_\infty^2}, \tag{4}$$

$$-\frac{i\alpha^2 c}{T_0}\hat{v} + \frac{i\alpha^2 U_0\hat{v}}{T_0} = -\frac{1}{\gamma M_\infty^2}\hat{p}_Y, \tag{5}$$

$$\frac{1}{T_0}\left[-ic\hat{T} + iU_0\hat{T} + \hat{v}T_{0Y}\right] + (\frac{\gamma-1}{\gamma})(ic\hat{p} - iU_0\hat{p}) = 0, \tag{6}$$

$$\hat{p} = T_0\hat{\rho} + \frac{\hat{T}}{T_0}. \tag{7}$$

The above may be reduced to two first-order equations, namely

$$\hat{v}_Y - \frac{U_{0Y}\hat{v}}{U_0 - c} = \frac{i\hat{p}}{\gamma M_\infty^2}\left[\frac{T_0 - M_\infty^2(U_0 - c)^2}{U_0 - c}\right], \tag{8}$$

$$\frac{i\alpha^2(U_0 - c)\hat{v}}{T_0} = -\frac{\hat{p}_Y}{\gamma M_\infty^2}. \tag{9}$$

The usual zero permeability on the wall condition ($\hat{v}(Y = 0) = 0$) is replaced by the following condition linking perturbation normal velocity to perturbation pressure, i.e.

$$\hat{v} - \Lambda\hat{p} = 0. \tag{10}$$

Focusing on the particular case of a freestream Mach number $M_\infty = 6$ the first phase of this work (see also the appended AIAA paper) extensively investigated the effects of altering Λ (which in general will be complex). It was found that values of Λ lying within the third quadrant were particularly effective at reducing maximum growth rates, especially that of the second mode of instability.

The central issue is then how to link these outer-flow features to the flow inside each microcavity. This is addressed below.

Disturbance flowfield inside each microcavity

As noted above, the early part of the study revealed the flow inside each microcavity to be fundamentally very slow (i.e. incompressible *and* viscous). This second phase of the work has been involved with developing a model to obtain some connection between the inner and outer flow regimes. The model that has been developed in this second phase builds upon the work of Duck [4] on oscillatory lid-driven cavities. The fundamentals of the model used inside each microcavity are as follows:-

- The flow is viscous and incompressible.
- The flow is two-dimensional.
- The usual permeability and no-slip conditions are imposed on the bottom and two sides of the cavity (which is assumed to be rectangular in shape).
- The flow is driven solely by the disturbance (time-harmonic) flowfield, i.e. the outer base-flow boundary layer has no direct effect on the microcavity flow (this approximation was suggested by the investigations in the first phase of the study).

- The forcing (through the time-harmonic component of the flow) comprises two components:
  - through forcing on the normal velocity on the upper boundary; generally this in the form:

$$v(x, y = H, t) = \frac{1}{2} v_{top} \sin(2\pi x) e^{-i\Omega t} + c.c., \tag{11}$$

  - through forcing on the tangential velocity on the upper boundary; generally this was imposed in one of two forms

Model (a):

$$u(x, y = H, t) = \frac{1}{2} u_{top} e^{i(-\Omega t + \phi)} + c.c., \tag{12}$$

Model (b):

$$u(x, y = H, t) = \frac{1}{2} u_{top} e^{i(-\Omega t + \phi)} \sin(\pi x) + c.c.. \tag{13}$$

Here v_{top} and u_{top} are both constants (the latter implying a uniform tangential velocity across the top of the cavity in the case of model (a), namely (12)). Note that here Ω is directly related to αc in the analysis of the outer flow.

It should be noted that (11) was chosen specifically such that $v = 0$ at $x = 0$ and $x = 1$ in line with the impermeability constraint away from the pores/microcavities, and note too the zero total mass flux into each cavity. (12) was chosen because of its simplicity, whilst (13) was chosen in order to satisfy the no-slip condition away from the pores. Defining a streamfunction ψ, such that $(u, v) = (\psi_y, -\psi_x)$, then the problem (formally) is therefore as follows:

$$-i\Omega \nabla^2 \psi_t - \frac{\partial(\psi, \nabla^2 \psi)}{\partial(x, y)} = \frac{1}{Re} \nabla^4 \psi. \tag{14}$$

In the above, non-dimensionalisation of lengthscales has been performed using the width of the cavity, and as a consequence $0 \leq x \leq 1$, and so the vertical scale is $0 \leq y \leq H$. Velocities are non-dimensionalised with respect to the normal velocity, v_{top} and this is also used in the definition of the microcavity Reynolds number, Re (along with the cavity width); time is non-dimensionalised with respect to the cavity width and v_{top}. It should be emphasised that in the experiments of Rasheed et al. [2] (the regime of interest), both the pore spacing and width were considerably smaller than the outer boundary-layer thickness.

Since numerically it was found in the first phase of the study that $\Im\{\alpha c\}$ was typically numerically small, as a first step in modeling the cavity flow we set $\Omega_i = 0$ (although of course from the point of view of the stability of the outer flow, the finiteness and sign of $\Im\{\alpha c\}$ is crucially important; note that $|\Im\{\alpha c\}| << 1$ is a feature common to many flow stability studies).

This being the case, the flow was then decomposed harmonically as follows (following Duck [4])

$$\psi(x,y,t) = \sum_{n=-\infty}^{\infty} \psi_n(x,y) e^{int}, \tag{15}$$

where, if Ω is taken to be real, then ψ_{-n} = complex conjugate$\{\psi_n\}$. It was also found useful to introduced the vorticity components, ζ_n defined as follows:

$$\zeta_n = \nabla^2 \psi_n. \tag{16}$$

Then (16) was used in conjunction with

$$-i\Omega n \zeta_n - \sum_{m=-\infty}^{\infty} \left(\frac{\partial \psi_m}{\partial x} \frac{\partial \zeta_{n-m}}{\partial y} - \frac{\partial \psi_m}{\partial y} \frac{\partial \zeta_{n-m}}{\partial x} \right) = \frac{1}{Re} \nabla^2 \zeta_n. \tag{17}$$

The appropriate boundary conditions are

$$\begin{aligned} \psi_n(0 \le x \le 1, y = 0) = \psi_{ny}(0 \le x \le 1, y = 0) = \psi_n(x = 0, 0 \le y \le H) &= \\ \psi_{nx}(x = 0, 0 \le y \le H) = \psi_n(x = 1, 0 \le y \le H) = \psi_{nx}(x = 1, 0 \le y \le H) &= 0, \end{aligned} \tag{18}$$

whilst on the top ($y = H$): if $n \neq \pm 1$:

$$\psi_n(0 \le x \le 1, y = H) = \psi_{ny}(0 \le x \le 1, y = H) = 0, \tag{19}$$

but for $n = \pm 1$ then:

$$\psi_{\pm 1}(0 \le x \le 1, y = H) = \frac{1}{2} \left(\cos(2\pi x) - 1 \right), \tag{20}$$

and in the case of model (a):

$$\frac{\partial \psi_{\pm 1}}{\partial y}(0 \le x \le 1, y = H) = \frac{1}{2} \frac{u_{top}}{v_{top}} e^{\pm i\phi}, \tag{21}$$

whilst in the case of model (b):

$$\frac{\partial \psi_{\pm 1}}{\partial y}(0 \le x \le 1, y = H) = \frac{1}{2} \frac{u_{top}}{v_{top}} e^{\pm i\phi} \sin(\pi x). \tag{22}$$

The system (15) was truncated (at $n = \pm N$, where typically $N = 4$ was adequate for acceptable accuracy) and then solved using a (second-order) finite-difference approach; although these are well known for losing stability at higher Reynolds numbers (Re), this is not an issue in the parameter regimes of interest, and equally the accuracy in such regimes is perfectly adequate, on relatively modest grids.

The final (and key) step is then the determination of Λ (or its equivalent) in (10). In the previous study of Fedorov et al [3] (in which the flow details inside each microcavity were not considered in the same detail as the present study, with each cavity being assumed to be of infinite depth), an averaging process was implemented. Here we follow a similar idea, although the particular details are somewhat different. For the purposes of determining the coupling between the wall normal velocity and the pressure, we focus on just the primary ($n = \pm 1$) modes. The system (16) together with (17) admits the following symmetries:

$$p_{2n+1}(\frac{1}{2} - x, y) = -p_{2n+1}(x - \frac{1}{2}, y), \quad \psi_{2n+1}(\frac{1}{2} - x, y) = \psi_{2n+1}(x - \frac{1}{2}, y), \tag{23}$$

$$p_{2n}(\frac{1}{2} - x, y) = p_{2n}(x - \frac{1}{2}, y), \quad \psi_{2n}(\frac{1}{2} - x, y) = -\psi_{2n}(x - \frac{1}{2}, y). \tag{24}$$

Here p_n denotes the n^{th} pressure mode. First an averaging process was performed across the top of each cavity, to yield

$$\hat{\Lambda} = \int_0^1 \frac{-\psi_{1x}(x, y = H)}{p_1(x, y = H)} dx. \tag{25}$$

In order to evaluate p_1, first p_{1x} was determined from the x-component of the Navier-Stokes equations:

$$p_{1x} = -i\Omega\psi_{1y} + \frac{1}{Re}\zeta_{1y} + \sum_{m=-\infty}^{\infty} \left(\frac{\partial \psi_m}{\partial x} \frac{\partial^2 \psi_{n-m}}{\partial y^2} - \frac{\partial \psi_m}{\partial y} \frac{\partial^2 \psi_{n-m}}{\partial y \partial x} \right). \tag{26}$$

The antisymmetry (23) then enables us to write

$$p_1(x, y) = \int_{\frac{1}{2}}^{x} \frac{\partial p_1}{\partial x} dx. \tag{27}$$

Finally the following was taken as an estimate for the coupling coefficient

$$\Lambda^* = \sigma \hat{\Lambda}, \tag{28}$$

where σ is a measure of the porosity of the surface, which is the fraction of the overall volume taken up by the pores; following Fedorov et al [3] we generally took $\sigma = 0.5$.

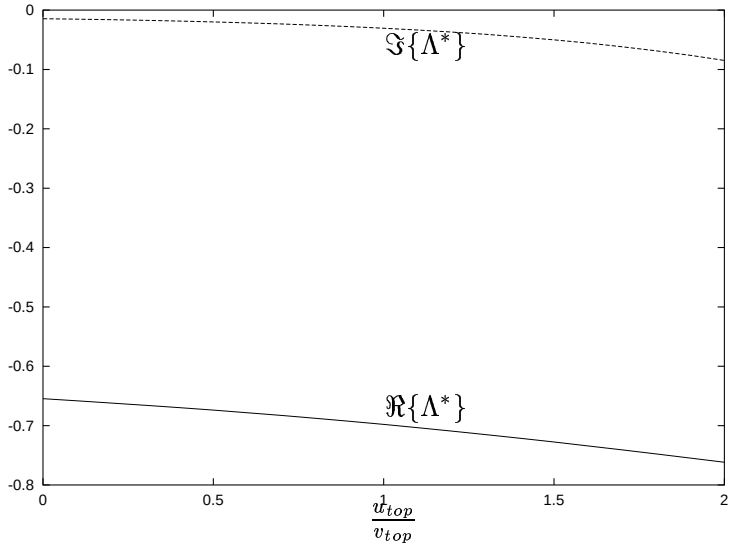

Figure 1: Singular case, $\Omega = 1$, $Re = 20$, $\phi = \pi/2$ (square cavity)

Results - model (a)

A number of calculations have been performed using this model. It should be noted that in this case a singularity on the top wall is provoked at $x = 0$ and $x = 1$, due to the discontinuity in x-wise velocity, in line with an identical form of singularity encountered in the classical steady lid-driven case of Burggraf [1].

A number of preliminary calculations were performed with various values of the phase shift parameter ϕ, with a view to determining the possibility of achieving values of the transpiration parameter Λ^* within the third quadrant - the zone found in the first phase of this work that produced the best reductions in growth rates of the second mode of instability (in particular). At an early stage it began very clear that this is indeed readily possible, and a useful choice of ϕ in this respect is $\phi = \pi/2$. For this reason, the results shown here will be confined to this particular choice, and emphasis will be place on the effect of varying the ratio $\frac{u_{top}}{v_{top}}$.

Figure 1 shows results for a square cavity ($H = 1$), at a Reynolds number $Re = 20$ and a frequency parameter of $\Omega = 1$. It is evident from these results that a increase in the parameter $\frac{u_{top}}{v_{top}}$ serves to increase the magnitude of both $\Re\{\Lambda^*\}$ and of $\Im\{\Lambda^*\}$, and is thereby likely to improve (in practical terms) the stability characteristics of the outer flow. This trend is repeated

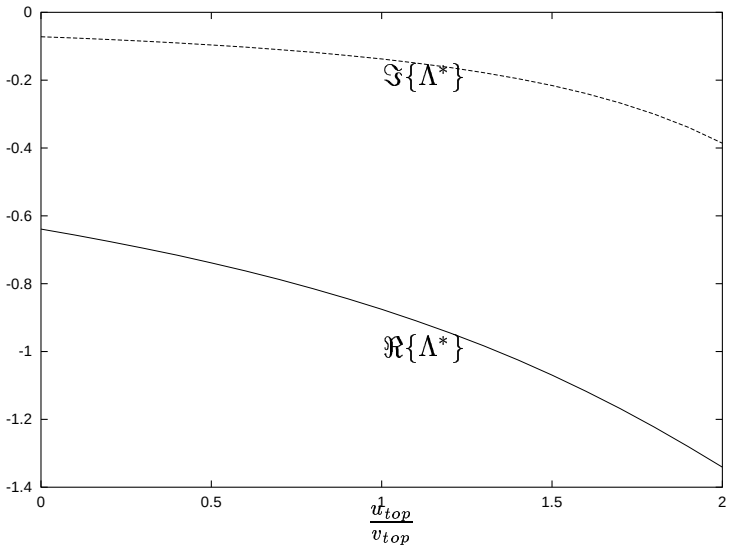

Figure 2: Singular case, $\Omega = 5$, $Re = 20$, $\phi = \pi/2$ (square cavity)

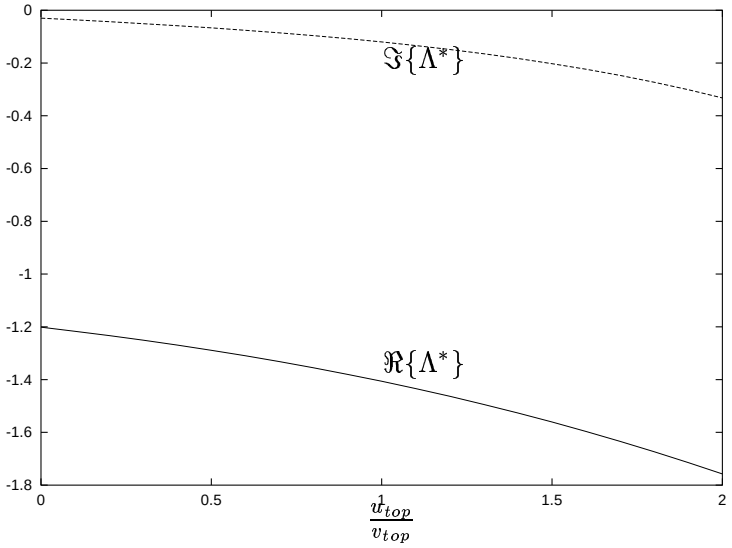

Figure 3: Singular case, $\Omega = 1$, $Re = 40$, $\phi = \pi/2$ (square cavity)

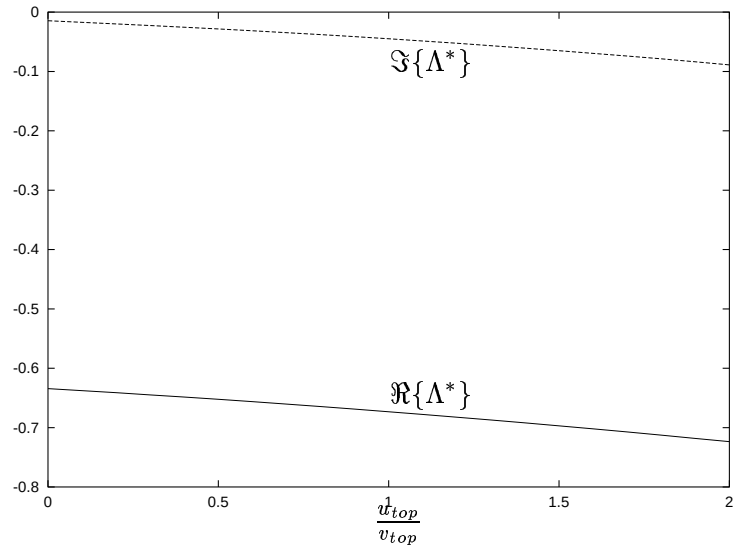

Figure 4: Singular case, $\Omega = 1$, $Re = 20$, $\phi = \pi/2$ (rectangular cavity, $H = 2$)

in the results shown in Figure 2 for which all parameters remain unchanged, except that the frequency parameter $\Omega = 5$ in this case. We see in these results a further encouraging trend, namely an increase in the magnitude of both $\Re\{\Lambda^*\}$ and of $\Im\{\Lambda^*\}$ (compared with the $\Omega = 1$ results), whilst this is observed again as $\frac{u_{top}}{v_{top}}$ increases. One important aspect here, with respect to the improvement with an increase in the value of the frequency parameter Ω is that in linking the outer flow regime to the microcavity flow regime, the net effect of scaling will be to increase the value of Ω in the microcavity flow regime. Yet another likely improvement in flow characteristics is to be observed in Figure 3; in this case, the parameters taken are a repeat of those in Figure 1, except that the Reynolds number $Re = 40$. In this case there is an approximate doubling of the magnitude of Λ^* (compared with the $Re = 20$ results).

Figure 4 show the results corresponding to Figure 1 but for the case of a cavity of aspect ratio two (i.e. $H = 2$, corresponding to a deeper cavity). What is particularly remarkable with these results ids that the results compare extremely closely with those for the unity aspect ratio case (i.e. $H = 1$) as depicted in Figure 1.

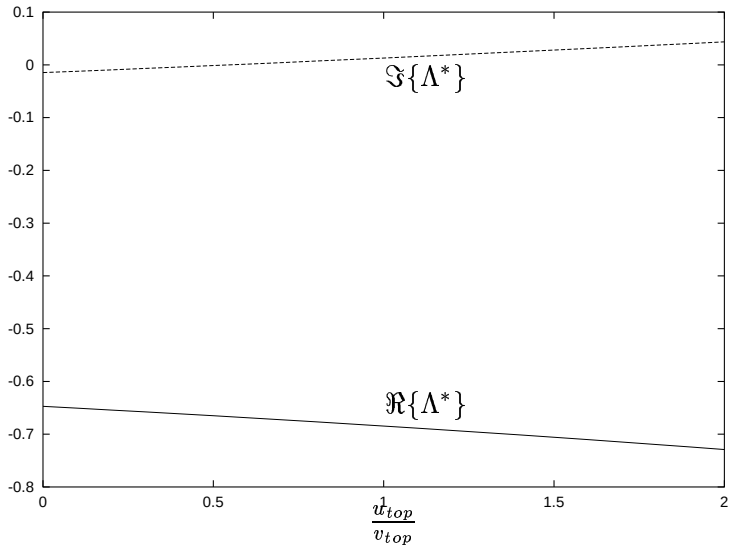

Figure 5: Regularized case, $\Omega = 1$, $Re = 20$, $\phi = \pi/2$ (square cavity)

Results - model (b)

In this case, because the x velocity component on the top boundary at $x = 0$ and $x = 1$ is zero, then the singularity encountered at these two locations with model (a) is no longer an issue (indeed, this type of approach is frequently referred to as the regularized problem).

Figure 5 shows results for a square cavity ($H = 1$) with a Reynolds number $Re = 20$ and a frequency parameter $\Omega = 1$ and (as in all previous results) a phase shift parameter $\phi = \pi/2$. There is evidence here of $\Im\{\Lambda^*\}$ becoming positive as the ratio $\frac{u_{top}}{v_{top}}$ is increased, although (again in practical terms) the net result of increasing this parameter is likely to still have beneficial consequences, on account of the increase in the magnitude of $\Re\{\Lambda^*\}$. Figure 6 corresponds to the case $\Omega = 5$ (all other parameters unchanged from Figure 6). In this case the results bear a very close resemblance to those presented above for the corresponding singular case (Figure 2). This in itself is encouraging, indicating a degree of universality, independent of our flow model. This observation is repeated in Figure 7, which repeats the calculation of Figure 2, but with the higher Reynolds number $Re = 40$; this indicates a good deal of similarity with the corresponding singular results presented in Figure 3.

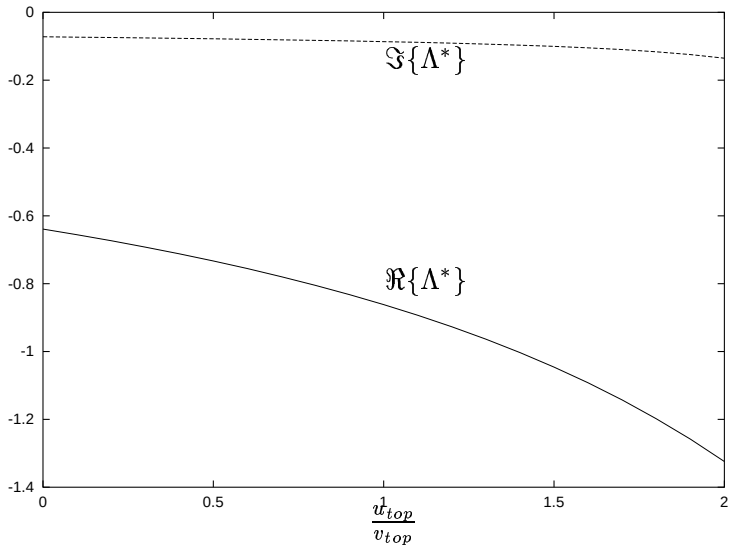

Figure 6: Regularized case, $\Omega = 5$, $Re = 20$, $\phi = \pi/2$ (square cavity)

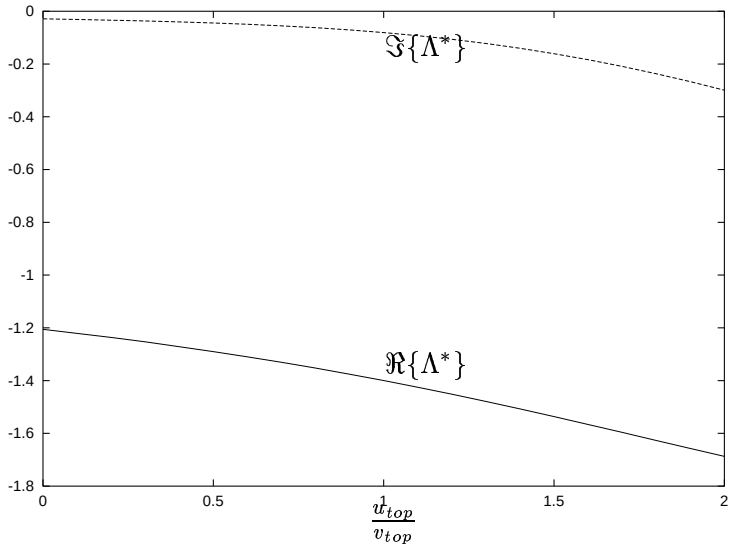

Figure 7: Regularized case, $\Omega = 1$, $Re = 40$, $\phi = \pi/2$ (square cavity)

3 Conclusions and future directions

This study has clearly indicated the feasibility of significantly stabilizing a hypersonic boundary layer through the use of microcavities. This effect is again seen to be robust - achievable over a broad regime of parameters (in particular from the results for the porosity parameters Λ (Λ^*) in our analysis), which indicates the potential for a real practical tool in laminar flow control.

One particularly encouraging observation in our results is that there is a good deal of similarity between the results for the singular cavity (model (a)) and those for the regularized cavity (b)). The conclusion from this is then that there is some independence of results on modeling, adding credence to the results. A further positive feature of the study is the indication that the results are quite independent of the dimensions of the microcavity (compare Figure 1 for a unit aspect ratio cavity with Figure 4 for an aspect ratio of two). This again points to the desired effects of the porous surface being achievable without the need for delicate fine tuning of the wall surface characteristics.

The results presented in this report suggest that an improvement may be achieved in outer flow stability characteristics with the following:

- An increase the in frequency parameter Ω; as noted already, the 'matching' between the outer flow and the microcavity flow (taking into account the different scalings in these two zones) will certainly have this effect.

- An increase in the microcavity Reynolds number (Re), i.e. with an increase in the flow speed within the cavity (although this could obviously have a corresponding adverse effect on the boundary-layer flow).

- An increase in the ratio parameter $\frac{u_{top}}{v_{top}}$; indeed this is not incompatible with the comment above with regard to the Reynolds number.

On account of the significant number of physical parameters occurring in the full problem, only limited (albeit potentially important, interesting and useful) regions of parameter space have been explored; obviously a more detailed investigation could reveal other important effects, and a wider study could used in a more detailed optimization process in order to stabilise, as far as possible, the boundary-layer flow.

The modeling in this work has relied on a number of fundamental assumptions, and the potential exists for relaxing a number of these in turn.

One direction of significant interest would be to investigate the role of Stokes layers that must inevitably occur in the stability regime of interest. The stability analysis undertaken in this project has been based on *inviscid* stability analyses, which is entirely correct and appropriate in the hypersonic flow regime. However this analysis also requires the inclusion of thin Stokes layers very close to the body surface which (in mathematical terms) are responsible for ensuring the no-slip condition is satisfied on the body surface. Inspection of the parameters in the experiments of Rasheed et al [2] reveal that the cavity dimensions are comparable to the thickness of the Stokes layers, and there therefore exists the potential for significant flow interaction between the microcavities and these Stokes layers.

A further effect that would be of great interest would be the cavity/cavity interaction. In the analysis performed to date, single, isolated microcavities have been the main focus of attention (although the the associated work of Theofilis, some attention has been directed at the interaction between just two cavities). This effect is certainly an area which could shed further significant light on the nature of the overall stabilization process.

References

[1] Burggraf, O.R. Analytical and numerical studies of the structure of steady separated flows. J. Fluid Mech. 24, 113 (1966).

[2] Rasheed, A., Hornung, H.G., Fedorov, A.V. and Malmuth, N.D. *Experiments on passive hypervelocity boundary-layer control using a porous surface.* AIAA paper 2001-0274.

[3] Fedorov, A.V., Malmuth, N.D., Rasheed, A. and Hornung, H.G. *Stabilization of hypersonic boundary layer by porous coatings.* AIAA paper 2001-0891.

[4] Duck, P.W. 1982 *Oscillatory flows inside a square cavity.* J. Fluid Mech. 122, 215

AIAA 2002–2987

FLOW AND FLOW INSTABILITY INSIDE A MICROCAVITY

Peter W. Duck
Department of Mathematics, University of Manchester, Manchester, M13 9PL, England

and

Vassilios Theofilis
DLR Institute of Aerodynamics and Flow Technology, Bunsenstraße 10, D-37073 Göttingen, Germany

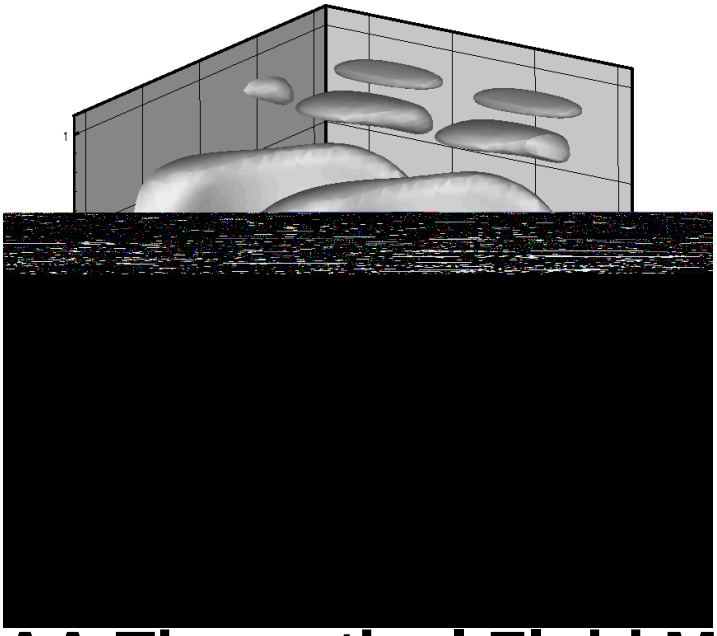

3rd AIAA Theoretical Fluid Mechanics Meeting

24 – 26 June, 2002 / St. Louis, MO

FLOW AND FLOW INSTABILITY INSIDE A MICROCAVITY

Peter W. Duck
Department of Mathematics, University of Manchester,
Manchester, M13 9PL, England

and

Vassilios Theofilis
DLR Institute of Aerodynamics and Flow Technology,
Bunsenstraße 10, D-37073 Göttingen, Germany

Recent theoretical and experimental investigations have suggested that the mode II instability in hypersonic boundary layers can be considerably stabilized by coating the wall surface with a porous material, effectively introducing an array of microcavities on this surface. This paper is concerned with two aspects of this problem. Firstly the flow inside a solitary microcavity is examined. Order-of-magnitude arguments lead to the conclusion that the flow inside each microcavity is likely to be not only incompressible, but also has a (local) Reynolds number which is modestly low; this is due to the small scale of the microcavities. Both the basic flow within a cavity and its stability are calculated in the light of this conclusion. Secondly the flow outside the microcavities is examined. A flat-plate hypersonic boundary layer is assumed for the basic state, and an (inviscid) stability analysis (which is certainly appropriate for mode II instabilities in the Mach number regime of interest) is performed. The porosity of the wall surface in modeled in the stability analysis by permeability. This indicates that it is extremely easy to halve disturbance temporal growth rates over a broad range of parameter values, thus indicating a potentially robust and hence useful means of flow stabilization.

Nomenclature

Latin Symbols

c	complex eigenvalue of the local linear instability analysis
d	cavity diameter
D	cavity depth
M	Mach number
Re	Reynolds number
$\mathsf{Re}_{\mathsf{int}}$	Reynolds number based on an integral length
S	cavity spacing
$(\bar{\mathsf{u}}, \bar{\mathsf{v}}, 0, \bar{\mathsf{p}})^{\mathsf{T}}$	basic flow velocity components and pressure
$(\mathsf{U}_0, \mathsf{T}_0)^{\mathsf{T}}$	basic flow velocity and temperature in the compressible boundary layer
$(\tilde{\mathsf{u}}, \tilde{\mathsf{v}}, \tilde{\mathsf{w}}, \tilde{\mathsf{p}})^{\mathsf{T}}$	disturbance flow velocity components and pressure
$(\bar{\mathsf{u}}, \bar{\mathsf{v}}, \bar{\mathsf{w}}, \bar{\mathsf{p}})^{\mathsf{T}}$	disturbance flow amplitude functions
$(\mathsf{x}, \mathsf{y}, \mathsf{z})^{\mathsf{T}}$	Cartesian coordinate system inside the microcavity
Y	transverse boundary-layer coordinate

Greek symbols

α, β	wave numbers in x, z directions
γ	ratio of specific heats
δ	boundary-layer thickness
Λ	wall permeability parameter
μ, ν	viscosity, kinematic viscosity
ρ	density of compressible fluid
ψ	stream-function of incompressible fluid
τ	shear stress
ζ	vorticity of incompressible fluid
Ω	complex eigenvalue of the linear instability analysis

Cal ematic visco a fi ter

This material is based upon work supported by the European Office of Aerospace Research and Development, Air Force Office of Scientific Research, Air Force Research Laboratory, under Contract Nos. F6177 -01-WE046 and F6177 -01-WE049 monitored by Dr. Steven Walker and Dr. John Schmisseur.

It has been recently shown by Fedorov et al.[2] theoretically and Rasheed et al.[6] experimentally that mode II instability, which prevails in hypersonic boundary-layer flow under a variety of environmental conditions, can be very effectively controlled passively by coating the surface on which the instability develops by a porous material. The key feature of this technology is the large disparity of scales between a typical mode II wavelength and the diameter d of each of the microscopic cavities on the coating, schematically depicted in Figure 1. One consequence is that the effect of an array of microcavities on the flow can be modeled by replacing the impermeability and temperature boundary conditions at the wall by alternative conditions which these previous authors derived partly under the assumption of infinitely deep cavities. While this approach provides a satisfactory first estimate of the effect of the coating on the flow,[2] potential for improvement of the performance of the coating exists through improved knowledge of the flowfield in the neighborhood of each individual microcavity, which would thereby permit optimizing the spacing S between the microcavities, together with the depth D of these cavities, both of which are currently chosen in an arbitrary manner. Experiments which will partly focus on this issue are underway in Novosibirsk, although their expensive nature suggests that prior guidance offered by analytical/numerical means would contribute to focusing the efforts on selected promising configurations. This work is aimed at providing the first estimate of the necessary information by numerical means, together with an improvement in our scientific understanding of the processes that occur inside each cavity. We consider two distinct aspects of the problem. The first aspect is concerned with developing a thorough understanding of the flow regime inside the microcavities themselves, in order that accurate flow modeling and stability analysis can be performed. The second aspect is a detailed investigation of the flow instabilities outside of the microcavities, i.e. the flow in the outer boundary layer. This study leads to some very interesting conclusions regarding the mimimization of growth rates, with obvious application to the practical problem which is the subject of this project. The ultimate goal will be to link the two flow regimes (that inside the microcavities with that outside) in order to predict the best conditions for flow stabilizations. Our results suggest that significant flow stabilization can be achieved, over a broad range of parameter space, indicating a significant and feasible practical tool.

2. Steady flow inside a microcavity

As a first step in developing a detailed model for use in conjunction with the (stability) analysis of the type described below, and also employed by Fedorov et al,[2]

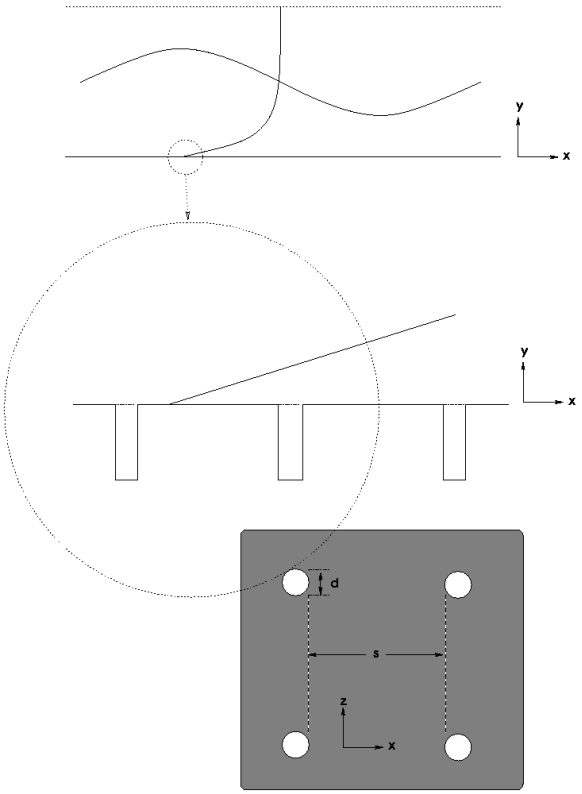

Fig. 1 Outline of the problem and definition of parameters

i.e. for use with the outer flow problem, we chose to consider the flow inside a single two-dimensional (micro)cavity. Recent work by Theofilis[8] and Theofilis, Duck & Owen[9] has considered the stability of the lid-driven flow inside a rectangular cavity which leads to a two-dimensional eigenvalue problem. In the model under consideration here, we again consider the basic flow to be that inside a rectangular, two-dimensional cavity, but with modified boundary conditions at the open end of the microcavity.

The theoretical aspects of the problem decompose naturally into two components: the basic flow within the cavity and the imposed, small amplitude, disturbance field. The former is calculated first, and then the details of this field are input into the determination of the latter. When considering the base flow, a reasonable starting point (given the spatial dimension parameters discussed below) is to impose impermeability together with uniform shear condition on the cavity roof; this implies that to leading order the outer flow is unaffected by the presence of the microcavities. On the other three cavity walls the usual no-slip and impermeability conditions are obviously appropriate. These latter conditions are clearly also entirely correct for the flow perturbations, whilst the condition appropriate on the roof of the cavity for the disturbance field is

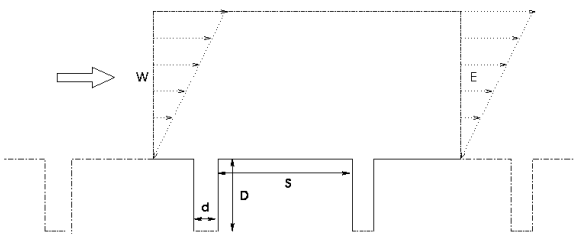

Fig. 2 Schematic representation of the minimal calculation domain encompassing two microcavities

less clear. Initially zero slip and impermeability would seem a good starting point, although at the next stage in the investigation, given the results to be described below, the impermeability constraint on the disturbance field may well be relaxed.

In the light of the remarks above, therefore, just a single cavity is considered in isolation - given the small scale of the cavity width ($60 \pm 4\mu$ m) compared with the separation between cavities ($100 \pm 7\mu$ m) in the experiments of Rasheed at al.[6] this would seen to be a reasonable first assumption; in turn, both these dimensions are considerably smaller than the local boundary-layer thickness in the outer flow. A further underlying simplification is that the basic flow field may be taken as being two dimensional, a procedure followed in the theoretical work of Fedorov et al.,[2] although the present study of this aspect does allow the consideration of three-dimensional imposed disturbances, with a harmonic decomposition in the spanwise, i.e. homogeneous direction. The key physical parameters are M_∞, the freestream Mach number, the thickness of the incoming boundary layer δ (which is uniquely related to the free-stream velocity U_∞) one length (e.g. S defined in Figure 2) and the length ratios d/D and d/S, as well as fluid viscosity μ. In brief, therefore, the basic flow model is that of flow inside a rectangular cavity, with no-slip/impermeable sides and base, with an impermeable top with an imposed shear stress. With this model it will be possible to refine and relax a number of the above assumptions.

Of paramount importance to the theoretical work is that the size of the microcavities is such that we may expect that the velocity inside the cavity to be small, in spite of the hypersonic nature of the external flow. This has two, key implications: firstly the Reynolds numbers based on the microcavity geometry are quite small (indeed the scale of the cavity width reinforces this); secondly, we certainly expect that the flow inside the cavity will be effectively incompressible (although temperature variations could be progressively introduced into the proposed model at a later stage). Let us be more specific, since these are crucial points. In particular, suppose we take the wall shear stress of the outer flow to be $\tau_w = \mu_w \frac{\partial u}{\partial y}|_w$, then we may expect freestream and wall values respectively. If the cavity (basic) flow is triggered in non-dimensional terms with a shear stress of unity, then matching this quantity inside the cavity with the external (wall) value leads us immediately to the conclusion that a typical velocity inside the cavity is $U_{cavity} = \frac{d}{\delta} U_\infty$, i.e. $\frac{d}{\delta}$ times the freestream value. In the results of Fedorov et al.,[2] this translates to a cavity/freestream ratio of $O(0.06)$; this in fact assumes that the typical cavity basic flow velocity is $O(1)$ with the imposed unity roof shear stress, but the basic flow calculations performed indicate that this turns out to be considerably smaller, further validating our argument. The repercussions for the Reynolds number are even more startling, and lead to the conclusion that the typical cavity Reynolds number (based on width) is $O(\frac{d^2}{\delta^2})$ that of the freestream. In practical terms, taking the Fedorov et al.[2] parameters, this translates to a factor $O(0.0036)$ times that of the external flow or a Reynolds number of $O(14)$ taking their case of an external value of 4000. This strongly suggests that the Fedorov et al.[2] approach of using inviscid theory to predict the behavior of the flow inside each cavity may not be sufficient - our order-of-magnitude arguments suggest a very viscous cavity flow.

A number of simplifications can be employed in order to gain first insights into the configuration at hand. Those pertaining to the external boundary-layer flow are discussed below; here we concentrate on the simplifications of the flowfield inside the microcavities. These amount to neglecting the three-dimensionality of the geometry for the purposes of the present effort as far as the basic state is concerned. Regarding global instabilities, a Fourier decomposition of the spanwise spatial direction is considered. As has been mentioned, it has been argued that flow inside the microcavity is essentially incompressible driven by constant shear, which leaves two parameters to be considered besides Reynolds number, namely the length over the depth of each microcavity and the spacing between two neighbouring microcavities. In the absence of prior information on the flow at hand, here we focus on the basic state inside a single microcavity and its global instability. The latter is contrasted with that in the classic lid-driven cavity.[8] Along the N-boundary of the integration domain uniform shear has been imposed, while no-slip conditions have been used on the solid walls to close the problem.

The basic flow is calculated by numerical solution of the vorticity transport equation alongside the relation between streamfunction and vorticity,

$$\frac{\partial \zeta}{\partial t} + \left\{ \frac{\partial \psi}{\partial y}\frac{\partial \zeta}{\partial x} - \frac{\partial \psi}{\partial x}\frac{\partial \zeta}{\partial y} \right\} - \mathcal{K}\zeta = 0, \quad (1)$$

$$\mathcal{K}\psi + \frac{1}{Re}\zeta = 0, \quad (2)$$

$\partial\bar{v}/\partial x$ is the vorticity of the basic flow and ψ is its streamfunction, for which $\bar{u} = \partial\psi/\partial y$ and $\bar{v} = -\partial\psi/\partial x$ holds. An accurate and efficient direct numerical simulation algorithm for the solution of (1) - (2) is presented in the next subsection.

The linear disturbance equations governing the global linear eigenvalue problem are obtained by substituting a decomposition into two-dimensional $O(1)$ basic quantities $\bar{\mathbf{q}} = (\bar{u}, \bar{v}, 0, \bar{p})^{\mathrm{T}}$ and three-dimensional $O(\varepsilon)$ disturbance quantities $\tilde{\mathbf{q}} = \hat{\mathbf{q}}(x, y)\mathrm{e}^{\mathrm{i}\,\{\beta z - \Omega t\}}$, with $\hat{\mathbf{q}} = (\hat{u}, \hat{v}, \hat{w}, \hat{p})^{\mathrm{T}}$ into the equations of motion, subtracting out the basic flow terms and neglecting terms at $O(\varepsilon^2)$. In the present temporal framework we take β to be a real wavenumber parameter describing an eigenmode in the $z-$direction and solve for the complex eigenvalue Ω. $\Omega_{\mathrm{r}} \equiv \Re\{\Omega\}$, the real part of the eigenvalue is related with the frequency of the global eigenmode while the imaginary part is its growth/damping rate; a positive value of $\Omega_{\mathrm{i}} \equiv \Im\{\Omega\}$ indicates exponential growth of the instability mode $\tilde{\mathbf{q}}$ in time t while $\Omega_{\mathrm{i}} < 0$ denotes decay of $\tilde{\mathbf{q}}$ in time. When the wavenumber vector is perpendicular to the plane on which the basic flow $(\bar{u}, \bar{v}, 0, \bar{p})$ develops, as the case is in the present basic flow, it is possible to simplify the two-dimensional eigenvalue problem by rewriting it as one with real coefficients, which requires half the amount of storage compared with the standard form.[9] The absence of a basic flow z-velocity component in the linear operator in conjunction of the redefinitions

$$\tilde{\Omega} = \mathrm{i}\,\Omega, \quad \tilde{w} = \mathrm{i}\,\hat{w} \tag{3}$$

result in the following generalized real nonsymmetric partial derivative EVP after linearisation and subtraction of the basic-flow related terms,

$$\begin{aligned}
[\mathcal{M} - (\mathcal{D}_x\bar{u})]\,\hat{u} - (\mathcal{D}_y\bar{u})\hat{v} - \mathcal{D}_x\hat{p} &= \tilde{\Omega}\,\hat{u}, & (4)\\
-(\mathcal{D}_x\bar{v})\hat{u} + [\mathcal{M} - (\mathcal{D}_y\bar{v})]\,\hat{v} - \mathcal{D}_y\hat{p} &= \tilde{\Omega}\,\hat{v}, & (5)\\
+\mathcal{M}\tilde{w} - \beta\hat{p} &= \tilde{\Omega}\,\tilde{w}, & (6)\\
\mathcal{D}_x\hat{u} + \mathcal{D}_y\hat{v} - \beta\tilde{w} &= 0, & (7)
\end{aligned}$$

where

$$\mathcal{M} = (1/Re)\left(\mathcal{D}_x^2 + \mathcal{D}_y^2 + \beta^2\right) - \bar{u}\mathcal{D}_x - \bar{v}\mathcal{D}_y. \tag{8}$$

The ability to solve a real eigenvalue problem is essential as the Reynolds numbers increases, Indeed, this point has been clearly manifested in the literature in the difficulties encountered by the investigators who tackled the problem of linear instability in the classic lid–driven cavity to produce consistent results.

Numerical methods

The principles of the algorithm discussed in what follows can be applied to recover three two–dimensional velocity components or indeed a three–dimensional flowfield;[4] however, for simplicity we confine the present discussion to solutions of the system

main advantage of the velocity–vorticity formulation is that the continuity equation is exactly satisfied. However, the problem of imposition of boundary conditions within the framework of an overall efficient numerical solution algorithm remains. This is compounded by the fact that the number of points discretising the two spatial directions in the subsequent analysis cannot be increased at will; while interpolation of a basic flow solution obtained on a very large number of points onto a modest EVP grid is one possible option, it is more elegant to avoid the interpolation procedure altogether and seek an accurate basic flow solution on *the same* small number of discretisation points on which the subsequent global instability analysis is to be performed. This appears tailor–made for a spectral numerical solution approach;[1] in what follows we discuss a different solution based on an efficient real–space eigenvalue decomposition (EVD) algorithm.

Chebyshev polynomials have almost exclusively been used in the past in the context of spectral simulations of the time–accurate Navier–Stokes and continuity equations, mainly due to the availability of fast transform algorithms necessary for efficient time–integration. However, for the present problems we have not restricted ourselves to this class of orthogonal polynomials. Considerable freedom exists in the choice of the expansion functions and the associated collocation grids by using Jacobi polynomials $P^{(q,r)}$ for the discretization of both spatial directions; of course, $q = r = -0.5$ may be related to the Chebyshev– while $q = r = 0$ are the Legendre polynomials. Collocation derivative matrices for both Jacobi Gauss-Lobatto and equidistant grids can be constructed from first principles; if $(x_j,\ j = 0, \cdots, n)$ is the collocation grid chosen, the entries d_{ij} of the $(0:n)\times(0:n)$ first-order derivative collocation matrix $\mathcal{D}$, derived analytically from the interpolating polynomial, are

$$d_{ij} = \frac{\prod_{k=0}^{n}(x_i - x_k)}{(x_i - x_j)\prod_{k=0}^{n}(x_j - x_k)}, \quad i, j, k = 0, \cdots, n, \quad i \neq j \neq k, \tag{9}$$

$$d_{ii} = \frac{1}{\sum_{k=0}^{n}(x_i - x_k)}, \quad i, k = 0, \cdots, n, \quad i \neq k. \tag{10}$$

These formulae result in the well–known ones if the analytically known Chebyshev Gauss-Lobatto grid ($x_j = \cos j\pi/n,\ j = 0, \cdots, n$) is used.[1] Values of order m derivatives on the collocation grid x_j are obtained by $(\mathcal{D})^m$. As far as temporal discretization of (1) is concerned, the viscous nature of the problems in which we are interested introduces scales which dictate an implicit treatment of the linear term in this equation; the nonlinear term may be treated explicitly.

not resort to splitting and introduction of intermediate fields but rather address the governing equations directly the combination of Crank–Nicholson (CN) with second–order Adams–Bashforth (AB2) or Runge–Kutta (RK) schemes has been extensively used for the time–integration of the viscous and the convective terms, respectively.[1] However, the family of compact schemes proposed by Spalart, Moser and Rogers[7] (SMR) presents more accurate and more stable alternatives to the CN–AB2 algorithm although it does not require additional computational effort to the latter scheme. The SMR algorithm may be written in compact form as

$$q^{'''} = q^{''} + \Delta t\Big\{\mathcal{L}(\kappa q^{''} + \lambda q^{'''}) + \kappa_1 \mathcal{N}(q^{''}) + \kappa_2 \mathcal{N}(q^{'})\Big\}, \tag{11}$$

where the superscript denotes fractional time–step, $\mathcal{L}(q)$ and $\mathcal{N}(q)$ are, respectively, the linear and nonlinear operators in the problem to be solved and Δt is the time–step. The rationale behind the derivation as well as sample values of the constants $\kappa, \lambda, \kappa_1$ and κ_2 of a self–starting SMR algorithm may be found in Spalart *et al.*[7] The time–discretization of (1) using (11) delivers the following problem to be solved for (ζ, ψ) at each fractional time–step

$$\mathcal{M}_1 \; \zeta^{'''} = R, \tag{12}$$

$$\mathcal{M}_2 \; \psi^{'''} + \zeta^{'''} = 0, \tag{13}$$

where $\mathcal{M}_1 = \partial^2/\partial x^2 + \partial^2/\partial y^2 - Re/(\lambda \Delta t)$ and $\mathcal{M}_2 = \partial^2/\partial x^2 + \partial^2/\partial y^2$, subject to boundary conditions appropriate to the problem in consideration. R comprises the nonlinear and the terms arising from the discretization at previous fractional time–steps,

$$\begin{aligned} R &= -(\kappa/\lambda)\left[\frac{\partial^2}{\partial x^2} + \frac{\partial^2}{\partial y^2} - Re/(\kappa \Delta t)\right] \zeta^{''} \\ &+ (\kappa_1 Re/\lambda)\left(\psi_y^{''}\zeta_x^{''} - \psi_x{}^{''}\zeta_y^{''}\right) \\ &+ (\kappa_2 Re/\lambda)\left(\psi_y^{'}\zeta_x^{'} - \psi_x{}^{'}\zeta_y^{'}\right). \end{aligned} \tag{14}$$

The accuracy of the overall procedure clearly depends on the scheme utilised for calculation of the spatial derivatives. The spectral discretisation chosen introduces dense matrices and can only become competitive against other numerical approaches from the point of view of efficiency on account of the existence of a fast algorithm for the inversion of the implicit operators $\mathcal{M}_1$ in (12) and $\mathcal{M}_2$ in (13). While $\mathcal{M}_2$ is time–independent, the first implicit operator is a function of a CFL–controlled maximum permitted time–step Δt and needs to be inverted at every time–step. If one sacrifices the advantage of an adjustable time–step and keeps Δt fixed at a slightly

rithm may be constructed for the efficient solution of the incompressible two–dimensional Navier–Stokes and continuity equations in streamfunction–vorticity formulation.

Key papers on EVD algorithms are the work of Haidvogel & Zang[3] and that of Ku et al.[4] The first authors discuss the solution of Poisson's eq

On account of the homogeneous boundary conditions (15) on ψ (13) becomes

$$\sum_{i=2}^{m-2} M_{ki}\psi_{il} + \sum_{j=2}^{n-2} N_{lj}\psi_{kj} = - \zeta_{kl} - M_{k1}\psi_{1l} - N_{ln-1}\psi_{kn-1} - N_{l1}\psi_{k1} - M_{km-1}\psi_{m-1l}. \quad (18)$$

The boundary conditions (16) - (17) may be expressed using the discrete analoga X, Y and Y^2 of the collocation derivative matrices $\mathcal{D}_x$, $\mathcal{D}_y$, and $\mathcal{D}_y^2$, respectively, as given by (9) - (10). It follows that

$$\psi_{1l} = \sum_{i=2}^{m-2} \delta_{1i}\psi_{il} \quad , \quad \psi_{m-1l} = \sum_{i=2}^{m-2} \delta_{m-1i}\psi_{il} \quad (19)$$

$$\psi_{k1} = \bar{\kappa}_k + \sum_{j=2}^{n-2} \epsilon_{1j}\psi_{kj} \quad , \quad \psi_{kn-1} = \bar{\lambda}_k + \sum_{j=2}^{n-2} \epsilon_{n-1j}\psi_{kj}, \quad (20)$$

where $\bar{\kappa}_k$ and $\bar{\lambda}_k$ are used to impose the boundary condition on the roof of the microcavity,

$$\bar{\kappa}_k = \frac{-F_k Y_{0n-1}}{Y_{01}Y^2_{nn-1} - Y^2_{n1}Y_{0n-1}}, \quad \bar{\lambda}_k = \frac{F_k Y_{01}}{Y_{01}Y^2_{nn-1} - Y^2_{n1}Y_{0n-1}} \quad (21)$$

and the vectors $\delta_{1i}, \delta_{m-1i}$ and $\epsilon_{1j}, \epsilon_{n-1j}$ are known functions of the entries of X, Y and Y^2,

$$\delta_{1i} = \frac{X_{0m-1}X_{mi} - X_{mm-1}X_{0i}}{X_{01}X_{mm-1} - X_{m1}X_{0m-1}}, \quad (22)$$

$$\delta_{m-1i} = \frac{X_{m1}X_{0i} - X_{01}X_{mi}}{X_{01}X_{mm-1} - X_{m1}X_{0m-1}}, \quad (23)$$

$$\epsilon_{1j} = \frac{Y_{0n-1}Y^2_{nj} - Y^2_{nn-1}Y_{0j}}{Y_{01}Y^2_{nn-1} - Y^2_{n1}Y_{0n-1}}, \quad (24)$$

$$\epsilon_{n-1j} = \frac{Y^2_{n1}Y_{0j} - Y_{01}Y^2_{nj}}{Y_{01}Y^2_{nn-1} - Y^2_{n1}Y_{0n-1}}. \quad (25)$$

The essence of the EVD_4 algorithm is to diagonalise the $(0:m-4)^2$ matrix $\hat{M}$ and the $(0:n-4)^2$ matrix $\hat{N}$ whose entries are

$$\hat{M}_{ki} = M_{ki} + M_{k1}\delta_{1i} + M_{km-1}\delta_{m-1i}, \quad k,i = 0,\cdots,m-4, \quad (26)$$

$$\hat{N}_{lj} = N_{lj} + N_{l1}\epsilon_{1j} + N_{ln-1}\epsilon_{n-1j}, \quad l,j = 0,\cdots,m-4. \quad (27)$$

This is in contrast to the EVD_2 algorithm of Ku *et al*[4] where an $(0:m-2)^2$ matrix $\hat{M}$ and an $(0:n-2)^2$ matrix $\hat{N}$ arising from the imposition of Dirichlet data must be diagonalised. The Poisson problem (18) becomes

$$\hat{M}f_{kl} + f_{kl}\hat{N} = -\zeta_{kl} - \hat{N}_{l1}\bar{\kappa}_k - \hat{N}_{ln-1}\bar{\lambda}_k = r_{kl} \quad (28)$$

diagonalised using their eigenvalue decomposition

$$\hat{M} = (M^*)\mu^*(M^*)^{-1} \quad \text{and} \quad \hat{N} = (N^*)\nu^*(N^*)^{-1} \quad (29)$$

to yield

$$\mu^*(M^*)^{-1}f_{kl}(N^*) + (M^*)^{-1}f_{kl}(N^*) = (M^*)^{-1}r_{kl}(N^*). \quad (30)$$

As a consequence, instead of having to solve the $(m-3)\times(n-3)$ system of simultaneous equations (28) one solves the $(m-3)\times(n-3)$ algebraic equations $f^* = r^*/(\mu^* + \nu^*)$ for $f^* = (M^*)^{-1}f_{kl}(N^*)$, given $r^* = (M^*)^{-1}r_{kl}(N^*)$. The cost of the algorithm is a negligibly small fraction of the cost of a direct algorithm for the solution of the Poisson problem. This is documented in table 1 where memory and run-time requirements are shown for solution of (1) - (2) in the lid–driven cavity problem.

3. Results

Basic flow

We implemented the algorithm discussed in the previous section which was modified compared with that of Theofilis, Duck & Owen[9] by replacing the uniform tangential velocity of the cavity roof by that of uniform wall shear stress, as detailed. The issue of the singularity of the boundary conditions at the NE and NW corners of the cavity is thus absent in the present calculations and the time-accurate spectral collocation scheme utilized for the calculation of the basic flow demonstrates exponential convergence. Unlike the standard lid-driven cavity, in which the condition $\psi_y = 1$ is imposed at the N boundary and defines the effective flow Reynolds number, there is some ambiguity in the definition of a Reynolds number in the present case. The input Reynolds number may be regarded as $Re = \bar{u}_y(y = D)d^2/\nu$, given that in our approach the roof shear stress is constant (or $\psi_{yy} = 1$); here ν is the kinematic viscosity of the fluid. Two additional Reynolds numbers useful for closer comparisons with the standard lid-driven cavity problem may also be defined, namely an integral Reynolds number

$$Re_{\mathrm{int}} = \frac{1}{\nu}\int_{x=0}^{d} \bar{u}(x, y = D)\, dx, \quad (31)$$

as well as that based on the maximum streamwise velocity component attained at $y = D$,

$$Re_{\max} = \frac{1}{\nu}\max\{\bar{u}(x, y = D)\}. \quad (32)$$

While ν is a fixed parameter in the basic flow calculation code, $\bar{u}(x, y = D)$ is unknown *a priori* and is determined from the converged basic-flow field. Taking $d = D = 1$ basic flow results have been obtained using a rectangular grid comprising upwards of 96 collocation points per spatial direction. These have been

	SUN Sparc 10				NEC SX4			
	EVD		direct inversion		EVD		direct inversion	
grid	size (Mb)	time (sec)	size (Mb)	time (sec)	size (Mb)	time (sec)	size (Mb)	time (sec)
16^2	0.4	4.4	1.1	3.7	4.03	0.03	4.03	0.1
24^2	0.5	5.4	3.6	10.5	5.03	0.14	6.03	0.3
32^2	0.6	6.6	10.0	39.7	5.03	0.25	13.03	1.1
48^2	0.8	15.3	46.9	460.6	6.03	0.56	48.03	8.4
64^2	1.1	31.8	143.9	5203.5	6.03	1.08	140.03	40.7
96^2	1.8	143.3	(*)	(*)	8.03	2.48	680.03	417.4
128^2	2.8	523.1	(*)	(*)	8.03	4.41	(*)	(*)

Table 1 Comparison of memory and run-time requirements for a single solution of a two–dimensional Poisson equation using direct inversion and the EVD_4 algorithm on one processor of a workstation and a supercomputer. Asterisks denote that the respective problem does not fit in the available memory on the workstation or that it cannot be solved within the existing batch queue time–limit on the supercomputer.

compared against the classic lid-driven cavity flow, the Reynolds number in the latter case taken to be of $O(Re_{\rm int})$ in the former. As an example a comparison between the constant-shear and lid-driven basic states in terms of the streamfunction ψ, the velocity components $\bar{u} = \psi_y, \bar{v} = -\psi_x$ and the vorticity ζ is shown in Figure 3. The shear-driven cavity results have been generated using $Re = 6250$, which yields an effective Reynolds number of $Re_{\rm int} \approx 300$. Both sets of the first three quantities and the vorticity of the shear-driven flow are presented by ten isolines between zero and the respective maxima. The comparison points to a general qualitative agreement between the two model flows. That the input Reynolds number (Re) in the shear-driven case is substantially higher than $Re_{\rm int}$ shows how relatively ineffective the constant shear driving mechanism is. In anticipation of the parameter range necessary to produce globally unstable flows,[8,9] constant-shear basic states were obtained at substantially larger values of the unit Reynolds number, as shown in Figure 4. A monotonic increase of both $Re_{\rm int}$ and $Re_{\rm max}$ as $1/\nu$ increases can be seen. The extent to which the quantitative differences between the basic states modify the stability characteristics of the lid-driven cavity flow is examined next.

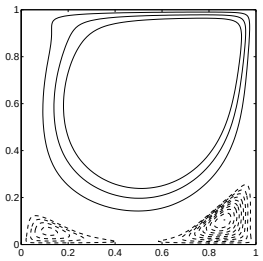

Global linear instability

In order to address the two-dimensional partial derivative eigenvalue problem appropriate boundary conditions must be specified. These are the straightforward viscous boundary conditions on the disturbance velocity components on the three solid walls while the issue of boundary conditions on the N boundary of the shear-driven cavity is expected to be the key to link the present configuration with that prevailing

of prior information, calculations reported here have been performed by imposing homogeneous Dirichlet or extrapolation of the disturbance velocity components from the cavity interior; appropriate compatibility conditions for the disturbance pressure have been used to close the system to be solved in both cases. In the framework of a temporal global instability analysis the only parameters of the problem are the flow Reynolds number Re and the spanwise periodicity length L_z, associated with a wavenumber $\beta = 2\pi/L_z$ while the complex temporal eigenvalue Ω and the two-dimensional amplitude functions $(\hat{u}, \hat{v}, \hat{w}, \hat{p})^{\mathrm{T}}$ of the disturbance quantities are determined by the numerical solution of the partial-derivative eigenvalue problem.

At $Re_{\mathrm{ldc}} = Re_{\mathrm{int}} \approx 300$ the lid-driven cavity flow is known to be stable to both two- and all three-dimensional perturbations. Comparisons between the two model flows are only possible in the case of homogeneous Dirichlet boundary conditions being imposed at the N boundary in the shear-driven case. The modification of the (least damped) leading eigenvalues of the eigenspectrum at $\beta = 7.5$ (approximately corresponding to least-damped conditions for mode T2[8, 9]) is shown in Figures 5 and 6. Owing to the disparity between Re_{ldc} and Re the shear-driven flow experiences much weaker damping compared with its lid-driven counterpart. Noteworthy is also the difference between the two flows in terms of the prevalence of stationary and low-frequency disturbances (in the neighbourhood of $\Omega_r = 0$) in the shear-driven cavity case at $Re = 6250$. At $Re = 25 \times 10^4$, on the other hand, the flow is marginally unstable at $\beta = 7.5$. The amplitude function of the spanwise disturbance velocity component $\hat{w}$ of the unstable global eigenmode is shown in Figure 7. The complexity of the (periodic in z) flowfield, setup by global instability inside the microcavity, can be seen in this figure, while the analogies of the structure of the global eigenmode with that in the lid-driven cavity can also be appreciated.[8, 9]

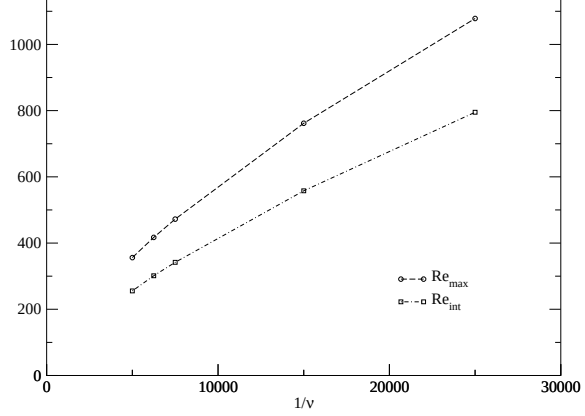

Fig. 4 Dependence of Re_{int} and $Re\mathrm{max}$ on $1/\nu$ in a square shear-driven cavity.

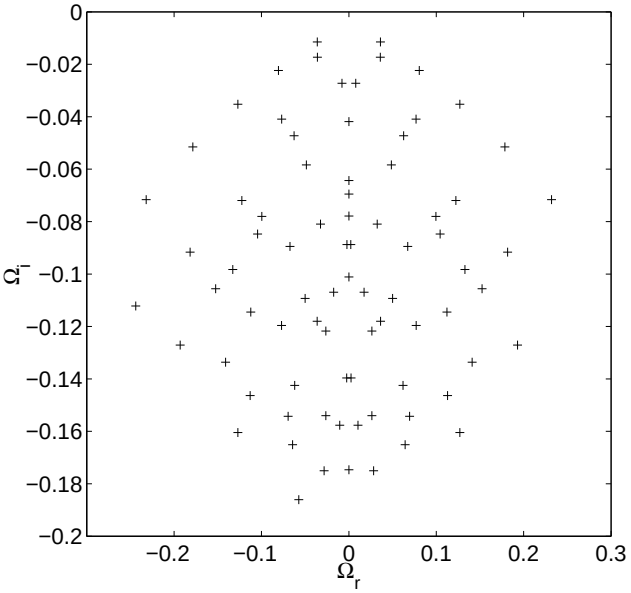

Fig. 5 Global eigenspectra in the shear-driven cavity.

4. The flow outside the microcavities

Turning our attention to the outer boundary layer flow next, the basic state in this region has been calculated using the standard compressible boundary-layer equations, together with the associated energy equation, assuming the similarity form appropriate for a boundary layer on a flat plate with zero streamwise pressure gradient. The Chapman viscosity law has been utilised; although this could easily be substituted for a more sophisticated model, our study indicates than any resulting differences, within the Mach number range considered, are minimal. Note also that the effects of shock waves have been ignored (indeed, this approximation was also employed by Fedorov et al.[2]). We note that the shock waves in the Mach number range of immediate interest are expected to lie well outside of the boundary layers, and that the flow disturbances of most interest are anticipated to be confined to well inside the boundary layers. Results for the base state are not presented here - these are well documented, and our results are entirely consistent with such previous work.

It is well known (Mack[5]) that an inviscid stability analysis of high-supersonic/hypersonic boundary layers

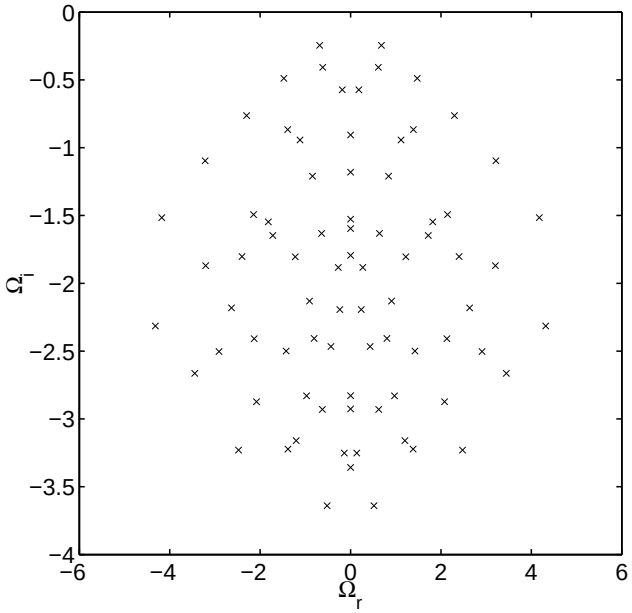

Fig. 6 Global eigenspectra in the lid-driven cavity.

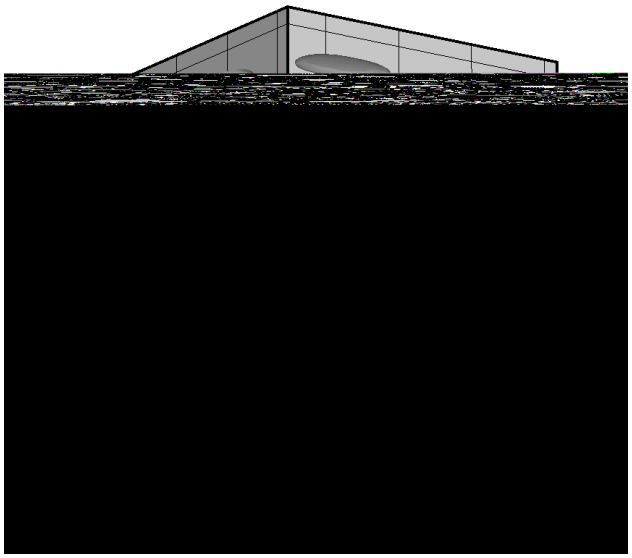

Fig. 7 Four isosurfaces of the spanwise disturbance velocity inside a square microcavity at ($Re = 25 \times 10^4, \beta = 7.5$). Levels are equidistributed between the minimum and maximum values.

tainly interested in here. We note that Fedorov et al.[2] did perform external stability calculations, using the full viscous disturbance equations, but the procedure adopted here, of using inviscid stability analysis permits many such calculations to be performed rapidly (on a PC/laptop computer), and thereby permits a thorough investigation of parameter space, and a subsequent optimization process to be performed efficiently.

Specifically, taking the x coordinate in the streamwise direction, Y the normal boundary-layer coordinate (scaled with $Re^{-\frac{1}{2}}$ in the usual boundary-layer manner), then the corresponding base flow (non-nondimensionalized with respect to the freestream velocity U_∞, which is also used in our definition of the Reynolds number Re), and temperature field, takes the form

$$(\mathbf{u}, T) = ((U_0(Y), 0), T_0(Y)) + O(Re^{-\frac{1}{2}}). \qquad (33)$$

Notice here the base flow is taken to be independent of the streamwise coordinate x – in reality such a locally parallel flow analysis is perfectly correct/justifiable if the (following) stability analysis is based on disturbances comparable to the boundary-layer thickness - this is certainly the case here.

We therefore decompose the perturbation flowfield in the following (normal-mode) manner

$$(\tilde{u}, \tilde{v}, \tilde{p}, \tilde{T}, \tilde{\rho}) = (\hat{u}, \hat{v}, \hat{p}, \hat{T}, \hat{\rho}) e^{iRe^{\frac{1}{2}}\alpha(x-ct)}, \qquad (34)$$

where $\tilde{u}$, $\tilde{v}$ and $\tilde{T}$, take on obvious meanings, $\tilde{p}$ and $\tilde{\rho}$ represent the perturbation pressure and density, respectively, and α denotes the wavenumber of the disturbance, c its wavespeed; the amplitude functions in the following *local* analysis are one-dimensional functions of the wall-normal coordinate Y, by contrast to the *global* analysis of the previous section, where the amplitude functions were defined on the two-dimensional plane of the microcavity. Note also that we are assuming a two-dimensional disturbance field - as shown by Mack this is the most 'dangerous' mode in this regime; however it is a simple matter to extend the analysis into the three-dimensional disturbance regime.

Substituting the disturbance flowfield into the inviscid, compressible equations of motion, discarding quadratic terms leads to the following system

$$-ic\hat{\rho} + \frac{i\hat{u}}{T_0} + \frac{1}{T_0}\tilde{v}_Y + iU_0\hat{\rho} + \hat{v}\frac{d}{dY}(\frac{1}{T_0}) = 0, \quad (35)$$

$$-\frac{ic}{T_0}\tilde{u} + \frac{iU_0\hat{u}}{T_0} + \frac{\hat{u}U_{0Y}}{T_0} = -\frac{i\hat{p}}{\gamma M_\infty^2}, \quad (36)$$

$$-\frac{i\alpha^2 c}{T_0}\hat{v} + \frac{i\alpha^2 U_0\hat{v}}{T_0} = -\frac{1}{\gamma M_\infty^2}\hat{p}_Y, \quad (37)$$

$$\frac{1}{T_0}\left[ic\hat{T} - iU_0\hat{T} - \hat{v}T_{0Y}\right] = (\frac{\gamma-1}{\gamma})(ic\hat{p} - iU_0\hat{p}), \quad (38)$$

$$\hat{p} = T_0\hat{\rho} + \frac{\hat{T}}{T_0}. \quad (39)$$

After some algebra it is possible to eliminate all but two of the dependent variables, and our choice was to work with the following system

$$\hat{v}_Y - \frac{U_{0Y}\hat{v}}{U_0 - c} = \frac{i\hat{p}}{\gamma M_\infty^2}\left[\frac{T_0 - M_\infty^2(U_0 - c)^2}{U_0 - c}\right], \quad (40)$$

$$\frac{i\alpha^2(U_0 - c)\hat{v}}{T_0} = -\frac{\hat{p}_Y}{\gamma M_\infty^2}. \quad (41)$$

In the usual, standard case of zero permeability on the wall the appropriate the boundary conditions are that $\hat{v}(Y = 0) = 0$, together with (generally) the disturbance field decays as $Y \to \infty$ *. However it is our assertion (which agrees with Fedorov et al.[2]) that the effect of the microcavities is primarily to modify this surface condition. We choose therefore to impose the following modified condition, which replaces impermeability with a relationship between normal velocity and pressure on the wall

$$\hat{v} - \Lambda\hat{p} = 0. \quad (42)$$

This is a reasonably general relationship, consistent with a well-posed solution of the above system. A numerical code was developed to solve the *temporal* eigenvalue problem, treating α as a real, specified parameter and evaluating the corresponding eigenvalue c. The method was based on a fourth-order solver, which has proved fast and effective on problems of this type in the past (Mack). In the case of neutral/stable disturbances, it is necessary to perform contour indentations (into the complex Y plane), and this was an integral part of the numerical code. A very thorough and detailed study was then made over a range of wavenumbers (α) and of surface parameter (Λ). Our results focus on the temporal growth rate $\Omega_i = \Im\{\alpha c\}$. Note there is no reason why Λ should necessarily be a real quantity, and so we therefore conducted a detailed study in complex Λ space, and we write $\Lambda = \Lambda_r + i\Lambda_i$. Further, in order to replicate the flow conditions studied by Fedorov et al.[2] and Rasheed et al.[6] all results shown here correspond to a freestream Mach number $M_\infty = 6$.

Figure 8 shows results for $\Lambda_i = 0$, for selected values of Λ_r; the case $\Lambda_r = 0$ therefore corresponds to the standard impermeable results (which can be checked against those of previous studies, for example Mack). In this standard case, the first and second modes of instability are quite distinct, and in line with the usual result that it is the second mode that dominates at these high Mach numbers. As Λ_r is reduced, however,

*There are some exceptional, neutrally stable cases where the disturbance is bounded as $Y \to \infty$ - we do not present details here, but we do note that our numerical scheme is well able to handle these.

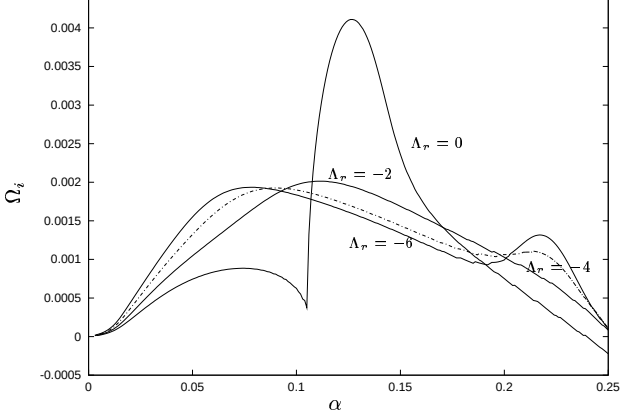

Fig. 8 $\Lambda_i = 0$

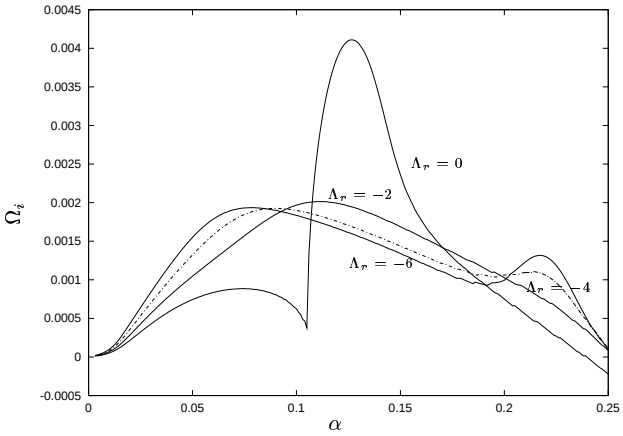

Fig. 9 $\Lambda_i = -1$

initially there is an amalgamation of the two modes, and also, crucially a marked reduction in maximum growth rate. In this case, the optimum choice of Λ_r (i.e. that exhibiting the least growth rate) is close to -4 and is shown as a dashed line (this is the convention we also use below to indicate near optimum conditions). Thereafter, i.e. as Λ_r is reduced still further, an increase in growth rates is observed at higher values of α (perhaps an increase in the significance of mode III) and this soon dominates and leads to a worsening of the stability characteristics. What is apparent, however, is that in this case, i.e. $\Lambda_i = 0$ it is very easy to get an approximate halving of maximum growth rate *over a very broad range of* Λ_r - this parameter does not require accurate or sensitive tuning to achieve this result.

Figure 9 shows the corresponding results when $\Lambda_i = -1$. There is a good deal of similarity displayed with those of Figure 8, although in this case it is the choice $\Lambda_r \approx -2$ that exhibits the lowest maximum growth rates; nonetheless an approximate halving of maximum growth rate is achieved again over a broad range

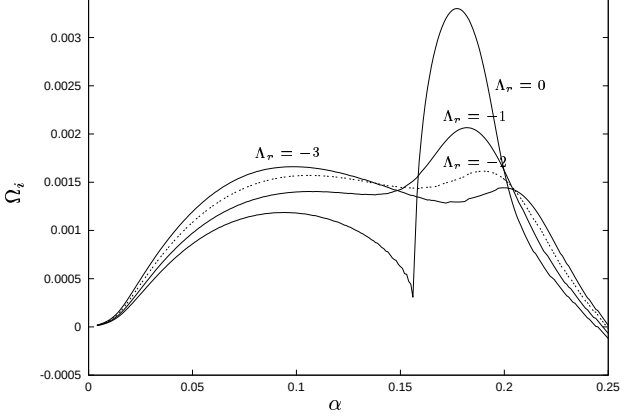

Fig. 10 $\Lambda_i = -2$

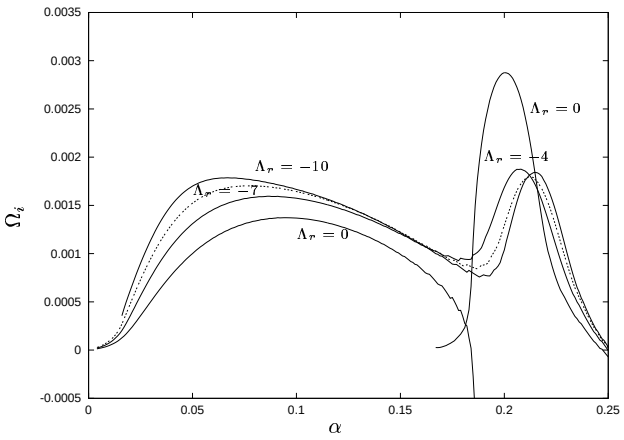

Fig. 11 $\Lambda_i = -5$

of Λ_r.

Results for $\Lambda_i = -2$ are displayed in Figure 10. In this case the optimum value of $\Lambda_r \approx -2$, but the results are otherwise in qualitative agreement with those of Figures 8 and 9. Results for $\Lambda_i = -5$ and $\Lambda_i = -10$ are shown in Figures 11 and 12, respectively, and exhibit optimum stability characteristics at $\Lambda_i \approx -7$ and $\Lambda_i \approx -12$ respectively. Remarkably, *all* our results illustrate how it is a simple matter to approximately halve maximum (temporal) growth rates over a wide range of choices of the parameter Λ. This strongly suggests this may be a useful and quite straightforward mechanism for outer flow stabilization.

5. Conclusions

In paper we have established the nature of the basic flow inside a cavity, driven by a uniform shear-stress on one face. This has been determined to be primarily viscous in nature, and thereby justifies the use of the (full) viscous *and incompressible* equations in this region, as employed in this paper. We do note that in the earlier work of Fedorov et al.[2] inviscid equations were used inside the microcavities (a detailed comparison will be made with this work in due course) although

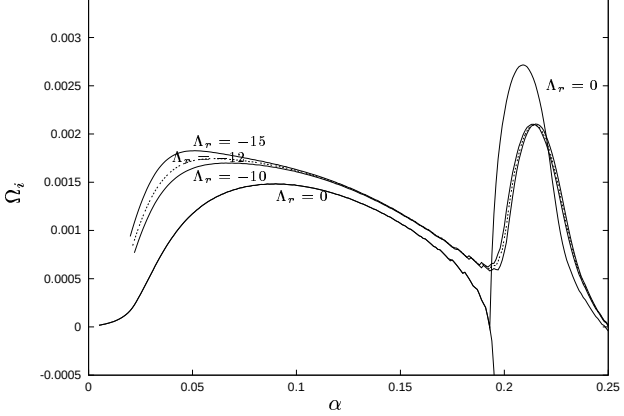

Fig. 12 $\Lambda_i = -10$

we may expect improved modeling of the flow using the more realistic (viscous) equations.

Some detailed stability analysis has also been performed on a boundary layer in a Mach 6 external flow. Using a modified surface boundary condition for this analysis to model the effects of the microcavities, it has been shown vividly that it is straightforward to obtain a halving of the maximum growth rates *over a very wide range of surface conditions.* This suggests a useful (and robust) tool for transition delay/prevention.

Future work will focus on use of the boundary condition at the open end of the microcavity as the key to relate flow instability inside the boundary layer with that inside the microcavity itself, in the continuing quest for hypersonic flow control through control of flow instability.

References

[1]Canuto C. Hussaini M.Y. Quarteroni A. and Zang T.A. 1987 *Spectral methods in fluid dynamics* Springer.

[2]Fedorov A.V. Malmuth N.D. Rasheed A. and Hornung H.G. 2001 *Stabilization of hypersonic boundary layer by porous coatings.* AIAA paper 2001-0891.

[3]Haidvogel D.B. and Zang T.A. 1979 *The accurate solution of Poisson's equation by expansion in Chebyshev polunomials* J. Comput. Phy. 39 167.

[4]Ku H.C. Hirsch R.S. and Taylor T.D. 1987 *A pseudospectral method for solution of the three-dimensional incompressible Navier-Stokes equations* J. Comput. Phy. 70 549

[5]Mack L.M. 1984 *Boundary-layer linear stability theory* in *Special course on stability and transition of laminar flow* AGARD Report No. 709 3-1

[6]Rasheed A. Hornung H.G. Fedorov A.V. and Malmuth N.D. 2001 *Experiments on passive hypervelocity boundary-layer control using a porous surface.* AIAA paper 2001-0274.

[7]Spalart P.R. Moser R.D. and Rogers M.M. 1991 *Spectral methods for the Navier-Stokes equations with one infinite and two periodic directions* J. Comput. Phys. 96 297.

[8]Theofilis V. 2000 *Globally unstable basic flows in open cavities.* AIAA paper 2000-1965.

[9]Theofilis V. Duck P.W. and Owen J. 2002. *Global viscous linear stability of three classes of rectangular duct flows.* Submitted to J. Fluid Mech.